The climates of Earth's next supercontinent: effects of tectonics, rotation rate, and insolation

Way, Michael; Davies, Hannah; Duarte, Joao; Green, Mattias

Geochemistry, Geophysics, Geosystems

26. Nov. 2023

The climates of Earth's next supercontinent: effects of tectonics, rotation rate, and insolation

M. J. Way[1,2,3], H. S. Davies[4,5], J. C. Duarte[4,5,6], and J. A. M. Green[7]

[1]NASA Goddard Institute for Space Studies, New York, USA
[2]Goddard Space Flight Center Sellers Exoplanet Environments Collaboration
[3]Theoretical Astrophysics, Department of Physics and Astronomy, Uppsala University, Uppsala, Sweden
[4]Instituto Dom Luiz (IDL), Faculdade de Ciências, Universidade de Lisboa, Lisbon, Portugal
[5]Departamento de Geologia, Faculdade de Ciências, Universidade de Lisboa, Lisbon, Portugal
[6]School of Earth, Atmosphere and Environment, Monash University, Melbourne, Victoria, Australia
[7]School of Ocean Sciences, Bangor University, Menai Bridge, UK

Key Points:

- The climate of a distant future Earth is modeled for two different supercontinent scenarios.
- Location and topographic height of the supercontinents are critical to mean surface temperatures assuming a modern Earth atmosphere.

Corresponding author: Michael Way, `michael.way@nasa.gov`

Abstract

We explore two possible Earth climate scenarios, 200 and 250 million years into the future, using projections of the evolution of plate tectonics, solar luminosity, and rotation rate. In one scenario, a supercontinent forms at low latitudes, whereas in the other it forms at high northerly latitudes with an Antarctic subcontinent remaining at the south pole. The climates between these two end points are quite stark, with differences in mean surface temperatures approaching several degrees. The main factor in these differences is related to the topographic height of the high latitude supercontinents where higher elevations promote snowfall and subsequent higher planetary albedos. These results demonstrate the need to consider alternative boundary conditions when simulating Earth-like exoplanetary climates.

Plain Language Summary

We investigate two tantalizing Earth climate scenarios 200 and 250 million years into the future. We show the role played by plate tectonics, the sun's increase in brightness, and a slightly slower rotation rate in these future climate scenarios. In one case the present day continents form into a single land-mass near the equator, and in the other case Antarctica stays put, but the rest of the present day continents are mostly pushed well north of the equator. The difference in the mean surface temperatures of these two cases differ by several degrees Celsius, while also being distinct in the total surface area in which they maintain temperatures allowing liquid water to exist year round.

1 Introduction

Earth's near-future climate has been extensively explored via the IPCC and associated CMIP studies (e.g. Collins et al., 2013). Earth's ancient climate has also been studied at various levels of detail, including the Cretaceous greenhouse (e.g., Huber et al., 2018), the Neoproterozoic Snowball (Pierrehumbert et al., 2011), and on the supercontinent Pangea (e.g., Parrish, 1993; Dunne et al., 2021). Some authors have explored Earths deep time future climate by looking at increases in CO_2, solar insolation through time (e.g., Sagan & Mullen, 1972) or looking at the future carbon cycle (e.g. Franck et al., 1999). Yet few have investigated climate effects induced by additional changes in topography and land/sea masks (e.g. Davies et al., 2018).

The geological formations on the ever-changing surface of the Earth have a strong influence on our climate. The transition to a cold climate in the Cenozoic, including the glaciation of Antarctica, was induced by opening of ocean gateways and reduced atmospheric CO_2 concentrations (Barker, 2001; DeConto & Pollard, 2003; Smith & Pickering, 2003). The development of the Caribbean arc and closing of the Panama Isthmus allowed the Gulf Stream to form, with major consequences for global climate (Montes et al., 2015), whereas the closure of the Strait of Gibraltar led to the Messinian Salinity Crisis (Krijgsman et al., 1999). Furthermore, the Himalayas, a consequence of the India-Eurasia collision, allows for the monsoon (Tada et al., 2016). Recently, Farnsworth et al. (2019) showed that the climate sensitivity for the period 150–35 million years ago is dependent on the continental configuration, particularly ocean area. Schmittner et al. (2011) investigated the effects of mountains on ocean circulation patterns of present day Earth and concluded that the current configuration of mountains and ice sheets determines the relative deep-water formation rates between the Atlantic and the Pacific Oceans.

The tectonic plates on Earth aggregate into supercontinents and then disperse on a cycle of 400-600 million years – the supercontinent cycle (Davies et al., 2018; Pastor-Galán et al., 2019; Yoshida, 2016; Yoshida & Santosh, 2018). The latest supercontinent Pangea formed around 310 million years ago and started breaking up around 180 million years ago. The next supercontinent will most likely form in 200–250 million years,

meaning Earth is currently about halfway through the scattered phase of the current supercontinent cycle (Davies et al., 2018).

There are obvious and strong links between large-scale tectonics and climate. It would be interesting to know what Earth's climate could be like in the distant future when continental movements will have taken Earth away from the current continental configuration (Davies et al., 2018). Here, we investigate what a climate may look like on Earth in a future supercontinent state. A secondary application of climate modelling of the deep-time future is to create a climate model of an Earth-like exoplanet using the parameters known to sustain habitability and a stable biosphere (Earth). Using the Deep-time future Earth as a basis for exoplanetary climate studies allows us to establish sensitivity ranges for the habitability and climate stability of the future Earth and its distant cousins in our galaxy.

2 Methods

2.1 Tectonic maps

Maps of the future Earth were produced based on two plausible scenarios for future Earth: Aurica (forming around 250 million years from now; Duarte et al., 2018) and Amasia (forming around 200 million years from now; Mitchell et al., 2012) – see Davies et al. (2018) for a summary. In both cases the ocean bathymetry was kept as in Davies et al. (2020), with continental shelf seas 150 m deep, mid-ocean ridges 1600 m deep at the crest point and deepening to the abyssal plains within $5°$, and subduction zones 6000 m deep. The abyssal plain was set to a depth maintaining the present day ocean volume. Each topographic file was generated with a $1/4°$ horizontal resolution in both latitude and longitude.

We generated three subsets of maps for each of the two supercontinent scenarios (see Table 1):

1. CTRL: Low mean topography (land close to sea level, 1–200 m), without mountains
2. PD: Higher mean topography (land close to present day mean topography, 1–4000 m) without mountains
3. MNTS: Low topography (1-200 m) with mountains (land close to sea level 1–200 m interspersed with mountains 2000–7000 m high)

The first subset of maps serve as a control (CTRL), allowing us to test the effect of the position and geometry of the continents without the influence of high topographies and particular features such as mountain ranges. It could also simulate a supercontinent that has existed long enough to have been almost fully eroded. The land here has been assigned topography with a normal distribution (mean = 1 m and standard deviation = 50 m) , giving topographic heights varying from 1 to 200 m.

The second set of maps assume mean topographic values close to those of present day (PD) but with no significant variation (e.g., no high mountains). This was made by applying a random topography following a normal distribution with mean and standard deviations closer to those of present day Earth's topography (i.e., mean of 612 m and standard deviation of 712 m). The resulting topography varies between 1 and 4000 m in height.

In the third set mountain ranges (MTNS) are included. The land of the supercontinent was first given a random topography similar to the control map (varying randomly between 1 and 200 m), after which mountains were added manually. The mountains are of three types: 1) Himalaya-type, which result from the collision of continents during the formation of the supercontinent, with an average peak elevation of 7500 m; 2) Andes-

Table 1. A summary list of the simulations & results.

Sim	Name	Topography	Ins[a]	LoD[b] (hrs)	Runtime (years)	T[c] (C)	Balance (Wm^{-2})	A[d] (%)	SnowFr[e] (%).	Hab[f] (%).
Aurica 250Myr into the Future										
01	Aurica	CTRL	1.0260	24.5	2000	20.5	0.2	30.5	0.5	1.000/1.000
02	”	PD	”	24.5	2500	20.6	0.1	30.1	0.6	0.955/0.956
03	”	MTNS	”	24.5	2000	20.6	0.2	30.3	1.5	0.974/0.983
Amasia 200Myr into the Future										
04	Amasia	CTRL	1.0223	24.5	3000	19.5	0.3	30.2	5.0	0.932/0.983
05	”	PD	”	24.5	3000	16.9	0.2	31.3	10.2	0.862/0.901
06	”	MTNS	”	24.5	3000	20.2	0.2	30.0	4.7	0.926/0.976
Modern Earth										
07	Earth_noAer_noO3		1.0	24.0	2000	13.5	-0.1	31.1	9.3	0.869/0.953
08	Earth_noAer_noO3_Rot		1.0	24.5	2000	13.3	0.2	31.0	9.5	0.865/0.951
09	Earth_noAer_noO3_Rot_Ins		1.0260	24.5	2000	17.7	-0.0	30.6	6.4	0.930/0.974

[a] Insolation, where 1.0 = 1361 W m^{-2} (Modern Earth).
[b] LoD = Length of Day in hours.
[c] Global mean surface temperature in degrees Celsius from an average over the last 10 years of the model run.
[d] Planetary Albedo.
[e] Snow and Ice, global fractional area.
[f] Habitable fraction (Spiegel et al., 2008) T>0/T>−15°.   3.

type, located at the margins of the continents along major subduction zones, with an average peak elevation of 4000 m; and 3) Appalachian-type, which correspond to eroded orogens that were formed and then partially eroded during the supercontinent cycle, with an average peak elevation of 2000 m. In all cases, the width of the mountains is 5° from peak to base.

2.2 Rotation changes

Day–length for the future was computed based on the simulated tidal dissipation rates presented in Green et al. (2018); Davies et al. (2019). The average dissipation during the remaining part of the supercontinent cycle is approximately half of the present day value (Green et al., 2018; Davies et al., 2019), leading to a change in day length that cannot be ignored. Consequently, we expect a change in daylength at approximately half the rate of present day, or about 1×10^{-3} s per 100 years (Bills & Ray, 1999) over the next 200 My. This leads to a day at the supercontinent state being ∼30 minutes longer than today, and this length of day (24.5 hours) was consequently used in all of the Future Climate General Circulation Model simulations discussed below.

2.3 General Circulation Model set up

The ROCKE-3D General Circulation Model (GCM) version Planet_1.0 (R3D1) as described in Way et al. (2017) is used for this study. A fully coupled dynamic ocean is utilized. Using data generated via Claire et al. (2012) we use an insolation value of $1361 \times 1.0223 = 1391.3$ W m^{-2} for the Amasia simulations (04–06) 200 Myr into the future. We use a value of $1361 \times 1.0260 = 1396.4$ W m^{-2} for the Aurica simulations (01–03) 250 My into the future. We do not change the solar spectrum as the changes for such a small leap into the future will be minimal in terms of its effect on the planet's atmosphere.

We use a 50/50 clay/sand mix for the soil given that we have no constraints on what the surface will be like in the deep future and is a value commonly used in the exoplanet community (e.g. Yang et al., 2014; Way et al., 2018). In a 3D-GCM the soil is important for its albedo and water holding capacity, see Section 2 of (Del Genio et al., 2019)
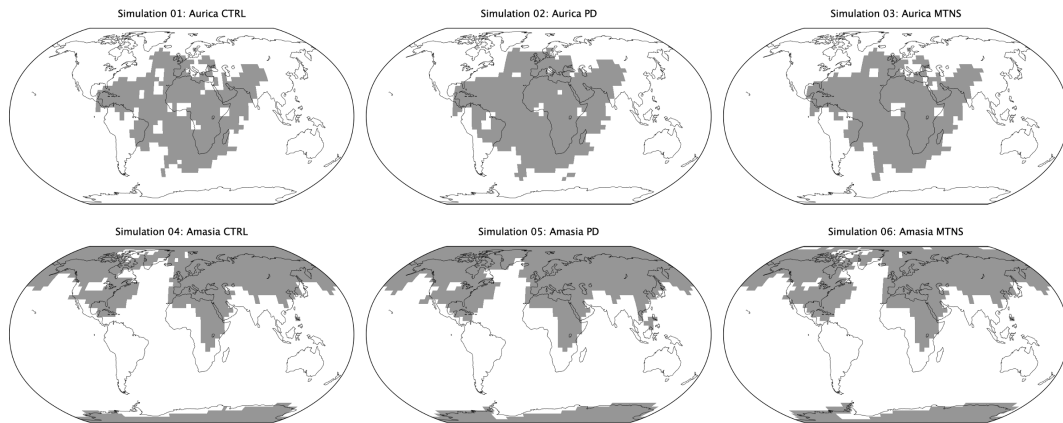
Figure 1. Land (grey) and Ocean/Lake (white) masks used in experiments of Table 1. Present day Earth continental outlines are shown for reference.

141 for details on the latter. 40 cm of water is initially distributed into each soil grid cell.
142 We use a ground albedo of 0.2 at model start, but the albedo will change via snow de-
143 position (brighter), or from rainfall (darker) as the GCM moves forward in time.

144   The original topography resolution of $1/4° \times 1/4°$ from the tectonic maps discussed
145 in Section 2.1 is down-sampled to a resolution of $4° \times 5°$ in latitude by longitude, which
146 is the default R3D1 resolution. The standard deviation from the down-sampling is used
147 to set the roughness length of the surface in each grid cell. River flow direction is based
148 on the resulting topography and exits to the ocean when possible. Large inland seas (typ-
149 ically less than 15 contiguous grid cells) are defined as lakes rather than ocean grid cells.
150 The GCM allows lakes to expand and contract as dictated by the competition between
151 evaporation and precipitation. The same holds for the possible creation and disappear-
152 ance of lakes. This allows the model to handle inland surface water in a more sophisti-
153 cated manner than making all surface water defined as ocean grid cells. This is highly
154 desirable because ocean grid cells cannot be created or destroyed during a model run.

155   Any ocean grid cell with a depth less than 150 meters (from the down-sampled $4° \times$
156 $5°$ data) was set to have a value of 204 meters (the mean depth of ocean model level 6).
157 This is especially important at high latitudes where shallow ocean cells may freeze to the
158 bottom causing the model to crash due to its inability to dynamically change surface types
159 from ocean to land ice.

160   The down-sampling has a side effect in that the land-sea mask will differ slightly
161 between the three topographic types (CTRL, PD, MTNS). For example, in a case with
162 a collection of ocean or lake grid cells adjacent to a number of high elevation land to-
163 pography grid cells the down-sampling may change the combined ocean + land grid cells
164 into a land grid cell, or vice-versa if the mean depth of the ocean grid cells is larger than
165 the height of the land grid cells. This is why the land/sea masks differ between CTRL,
166 PD and MTNS in Figure 1, even though their $1/4° \times 1/4°$ parents had exactly the same
167 land-sea mask.

168   One side-effect of having quite distinct land elevations and a lack of oceans in po-
169 lar regions in the Amasia runs (sims 04–06) is that snow accumulation can result in the
170 growth of ice sheets akin to that of Earth's last glacial maximum (LGM) when the Earth
171 was cooler than present day (Argus et al., 2014; Peltier et al., 2015). The increase in ice
172 sheet height can influence the climate as there may be substantially more snow accumu-
173 lation at higher elevations, whereas rain would normally fall at lower elevations, due to
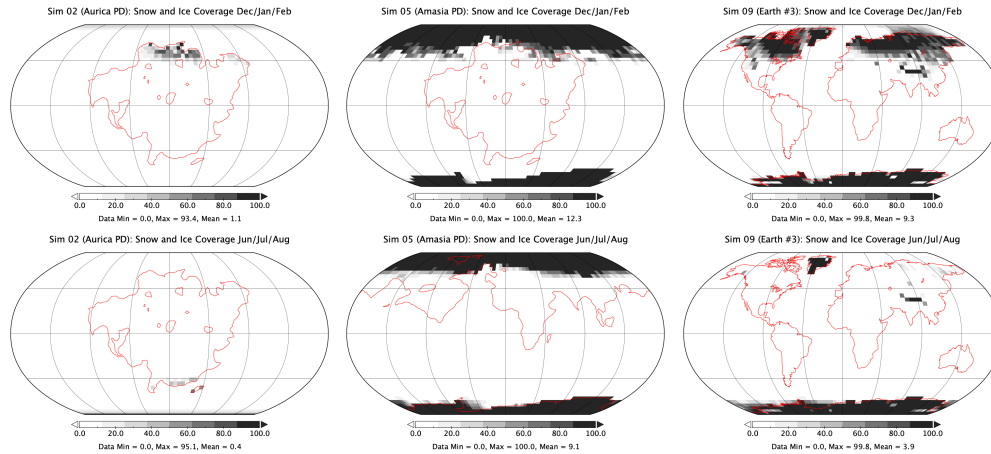
Figure 2. Individual grid cell snow+ice fractional amounts. For simulation 02 (left), simulation 05 (middle) and simulation 09 (right) for a 50-year climatological mean (from the last 50 years of each run) of the months of December, January and February (top) and June, July and August (bottom).

differences in the lapse rate. To accommodate this reality we ran models with the original Amasia topography (sims 04–05) and allowed snow to accumulate unhindered. Once these runs reached equilibrium we then used these snow accumulations as the bases for modified production runs. Fifty year climatological averages of snow accumulation (see Figure 2 middle panels) over N. Hemisphere summer months (June, July & August) was used to increase the elevations where necessary. We choose summer months since those minimum northern hemisphere accumulations work well to allow accumulation in the Fall/Winter months and evaporation in the Spring/Summer months. The same procedure is used in the southern hemisphere with 50 year climatological averages over the months of December, January & February. We then perform small areal averages over the highest latitudes to simulate the effect of ice sheet movement. These summer minima with snow accumulations are then labeled as permanent ice sheets (with appropriate albedo) in the model topography boundary condition files. We adopt this approach because R3D1 does not have a dynamic ice sheet model. An offline ice sheet model would be preferred as is typical in LGM studies (Argus et al., 2014; Peltier et al., 2015) but is beyond the scope of the present exploratory work. Figure S5 includes original topography plus snow accumulations (denoted as 'with ice sheets' in red dotted lines) versus the original topography (blue solid lines). For comparison purposes Figure S5d over plots the LGM data from Argus et al. (2014); Peltier et al. (2015). Recall that the LGM was at a time of lower solar insolation and differing orbital parameters from our future Earth scenarios. We believe that Figure S5d with the LGM over plotted demonstrates that our approach to dealing with the ice sheets is not unreasonable.

The atmosphere is set to roughly Earth constituents in the year 1850: Nitrogen dominated with 21% Oxygen, 285 ppmv CO_2, 0.3 ppmv N_2O, and 0.79 ppmv CH_4. No aerosols or Ozone (O_3) are included. For the minor species (CO_2 and CH_4) this is perhaps the simplest choice given the variability in the past (e.g. Ramstein, 2011), and long-term uncertainties associated with human generated climate change and the subsequent uncertainties associated with the long-term evolution of the carbon cycle (e.g., Franck et al., 1999). For the second most abundant species in Earth's atmosphere (O_2) the choice is consistent with recent estimates by Ozaki and Reinhard (2021) who set a 1σ limit of the longevity of Earth's 21% oxygenated atmosphere of $\sim 1 \times 10^9$ years. For comparison purposes with related work (Way et al., 2018) we include a modern Earth-like land/sea mask
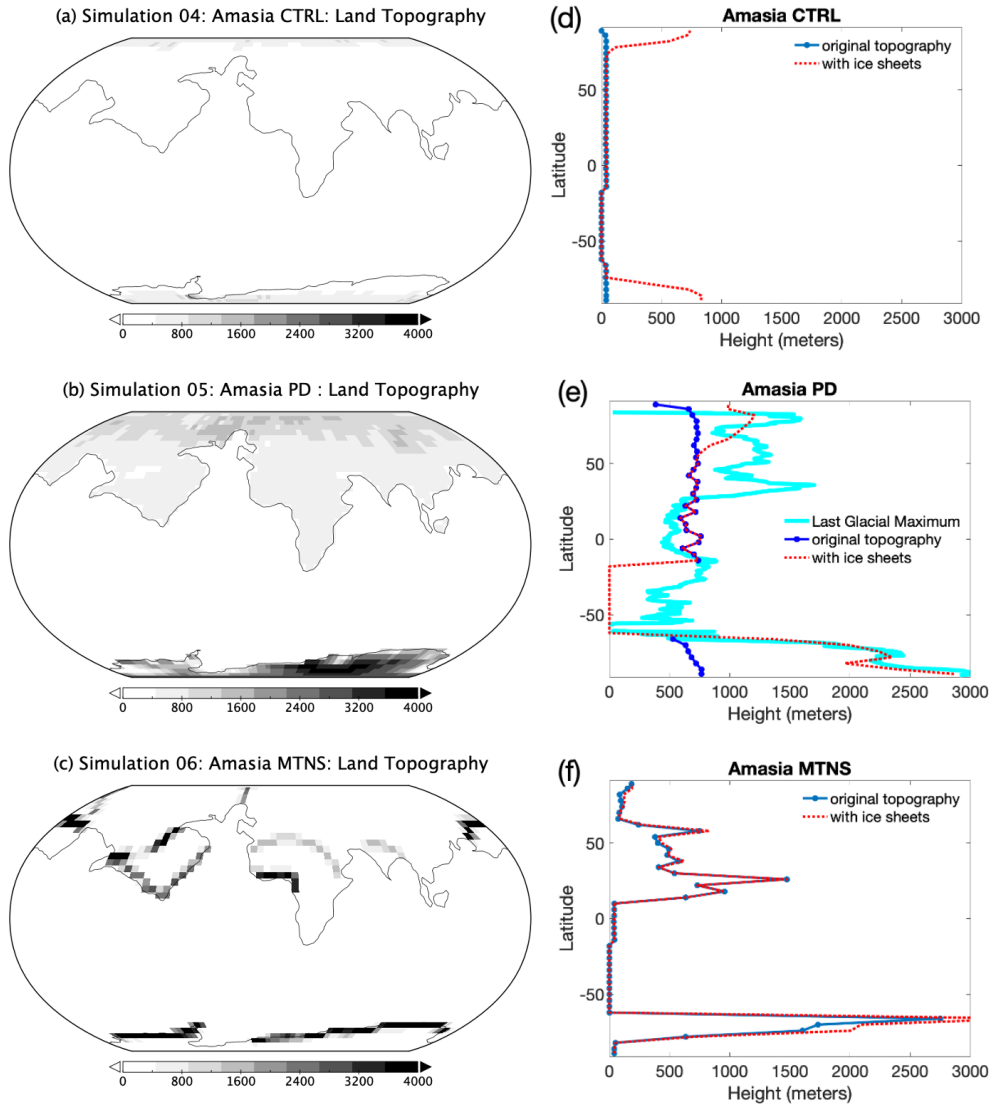
Figure 3. Amasia topography comparison: (a) Simulation 04 (Amasia CTRL): Area weighted mean height = 40 ± 11 m 'original topography.' 90 ± 30 m 'with icesheets,' (b) Simulation 05 (Amasia PD): Area weighted mean height = 702 ± 218 m 'original topography.' 921 ± 224 m 'with icesheets,' (c) Simulation 06 (Amasia MTNS): Area weighted mean height = 520 ± 542 m 'original topography.' 568 ± 593 m 'with icesheets,' d.) Simulation 04: Area weighted mean land height per latitude. e.) Simulation 05: Area weighted mean height per latitude for Sim 05 and Earth Last Glacial Maximum (cyan). f.) Simulation 06: Area weighted mean height per latitude.

in Simulations 07–09 (Table 1) with these same atmospheric constituents and a bath-tub ocean. The Earth-like land/sea mask used in these simulations is described in Way et al. (2018) and shown in Figure 8 of that paper. These changes do not greatly effect the mean surface temperature and make the model more resistant to crash conditions often associated with shallow ocean cells freezing to the bottom as would be likely in some of the cases herein. To better understand the possible effects of rotation rate and inso-lation (given such parameters used in Simulations 01–06) we take the same Earth model (Simulation 07) and slow the rotation rate (Simulation 08) to be the same as Simula-tions 01–06, and then increase the insolation (Simulation 09) to be the same as that of Simulations 01–03 as shown in Table 1 (the higher of the two insolations used at 200 and 250 Myr into the future).

3 Results

Let's first attempt to disentangle any effects of the slower rotation rate. We do this by looking at the modern Earth simulations (07–08). Table 1 shows a minimal differ-ence between the mean surface temperature between our Earth-like world with modern rotation rate (sim 07) and the 24.5 hour rotation for Sim 08 that is used by our Aurica and Amasia simulations (01–06). Planetary Albedo and snow+ice fraction are also nearly the same. In Figure S1a visible high latitude regional temperature differences ($\sim 5°C$) are seen between simulations 07 and 08 even if mean difference is only $0.2°C$.

Looking at Figure S2 (left panels) we see that simulations 07 and 08 also have very similar atmospheric, ocean and total meridional transport. If one compares the min and max stream functions in the tropics in Figure S3a and S3b (simulations 07 and 08) the differences are small: $-9.1 \times 10^{10}/-9.2 \times 10^{9} \sim 1\%$, $1.2 \times 10^{11}/1.19 \times 10^{11} < 1\%$.

Work by Showman et al. (2013, Figure 5) has shown that pole to equator temper-ature differences should decrease as rotation rate slows. There is a marginal difference at high northerly latitudes that in fact goes in the opposite direction (Figure S6a). With the slower rotating Sim 08 having a very small increase in equator-to-pole temperature difference. Note that the Showman et al. (2013) result is for much larger changes in ro-tation rate. Finally in Figure S6b we plot the eddy energy transport fluxes for simula-tions 07 and 08. One can see that the mid-latitude eddy energy flux in simulations 07 is slightly larger than that of 08, which would be consistent with that of Showman et al. (2013), but again the differences are marginal. In the end we find very little evidence that the additional 30 minutes in the length of day has any effect on the climate dynamics.

Next the rotation rate is fixed at 24.5 hours, but the insolation is increased from simulation 08 ($1361 =$ W m^{-2}) to simulation 09 ($1361 \times 1.0260 = 1396.4$ W m^{-2}). The differences are much clearer here with a $\sim 5°C$ difference in the mean surface tempera-ture. The planetary albedo has decreased $\sim 0.5\%$ which tracks the decrease in Snow+Ice fraction of $\sim 3\%$.

It should be noted that previous work has shown that some ancient Earth super-continent phases, which are comparable to our Aurica simulations 01–03, have had more arid interiors where weathering effects and CO_2 draw down may have been less efficient (e.g. Jellinek et al., 2019). This would increase surface temperatures as the balance of CO_2 would tend to be larger than present day because volcanic outgassing (sources) would likely remain constant while CO_2 drawdown (sinks) would decrease. However, there are other climatic effects to consider. For example, the Amasia reconstruction is essentially an arctic supercontinent with an independent and isolated antarctic continent, mean-ing both poles are covered by land, and much of that is covered by ice. Amasia is thus in essence a shift to consolidate the present day domination of northern latitude land masses even further north.

**(a) Sim 07 (Earth #1) − Sim 08 (Earth #2) Mean Surface Air Temperature**

Data Min = −2.1, Max = 5.4, Mean = 0.2
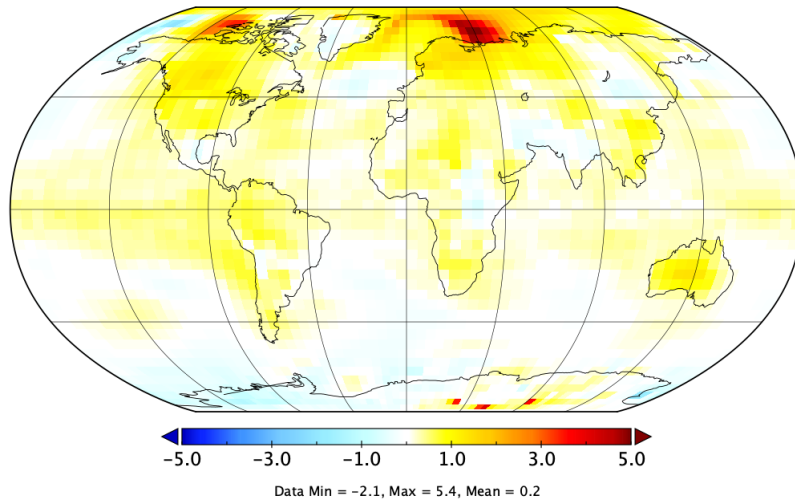
(b) Sim 09 (Earth #3) − Sim 08 (Earth #2) Mean Surface Air

Data Min = −0.7, Max = 16.2, Mean = 4.4
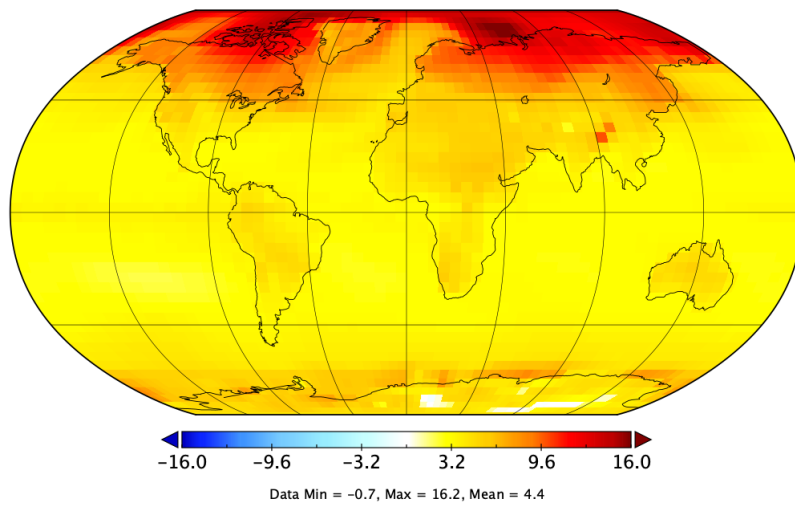
Figure 4. Differences in 10 year mean surface temperature (a) Simulation 07–08 and (b) 09–08. Note color bounds both straddle zero equally (cool blue colors below zero, zero white, yellows/reds above zero), but have different limits in each plot.
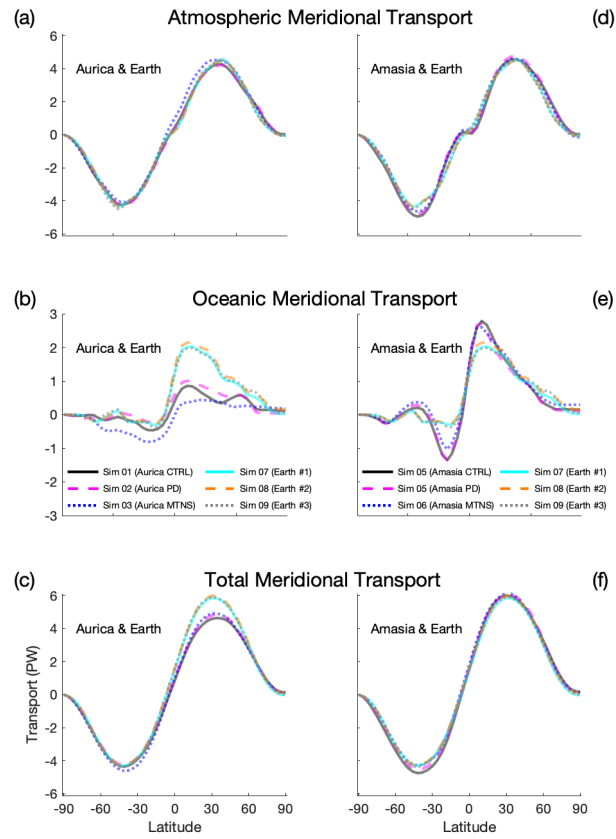
Figure 5. Atmospheric, Oceanic and Total Meridional Transport in PetaWatts (PW) $= 10^{15}$ Watts. Note that the ordinate limits for the middle panels are half those of the upper and lower panels to make the differences more readily discernible.
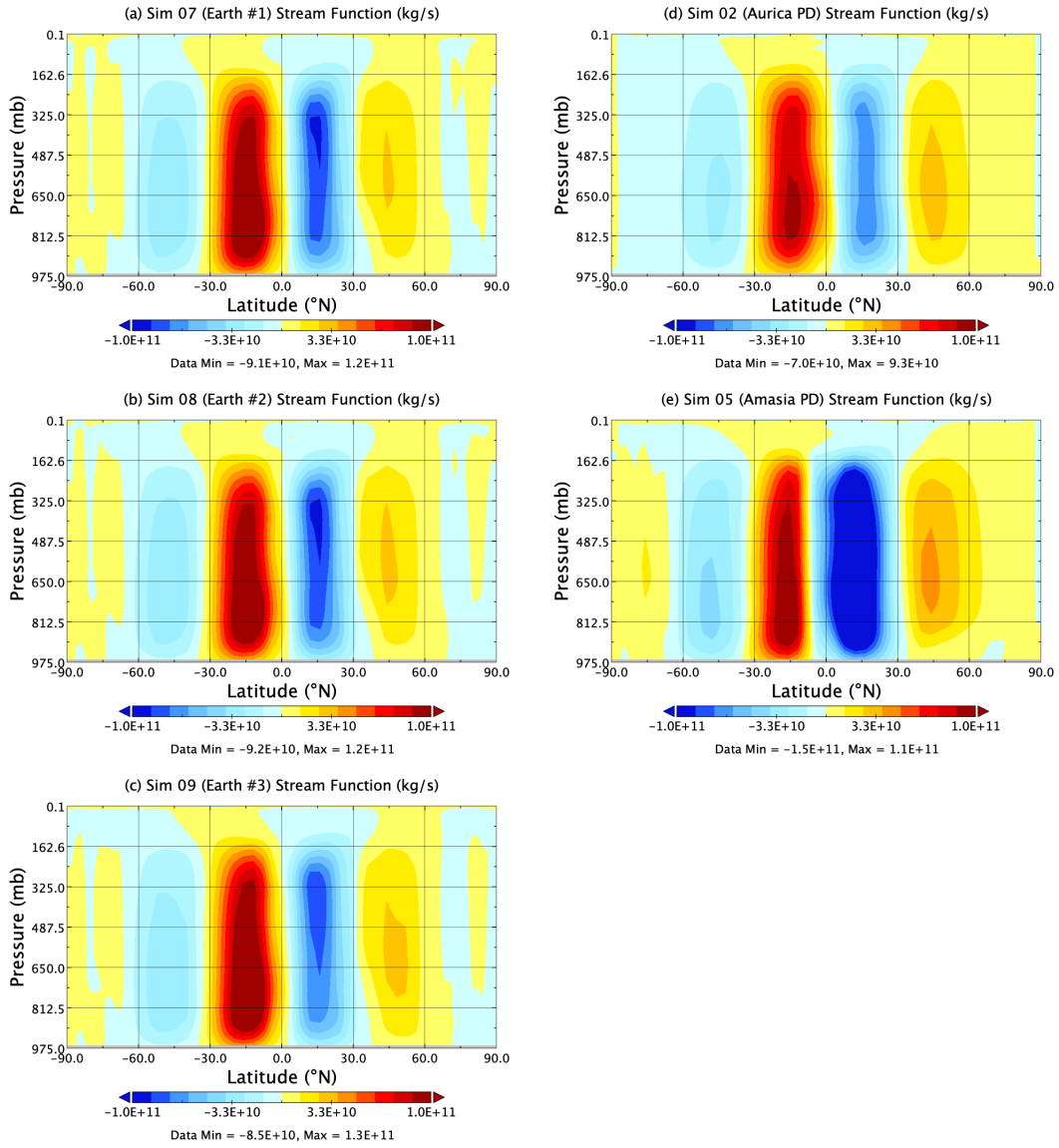
Figure 6. Stream Function for (a) Sim 07 (Earth_NoAer_noO3), (b) Sim 08 (Earth_NoAer_noO3_Rot), (c) Sim 09 (Earth_NoAer_noO3_Rot_Ins), (d) Sim 02 (Aurica PD), (e) Sim 05 (Amasia PD).
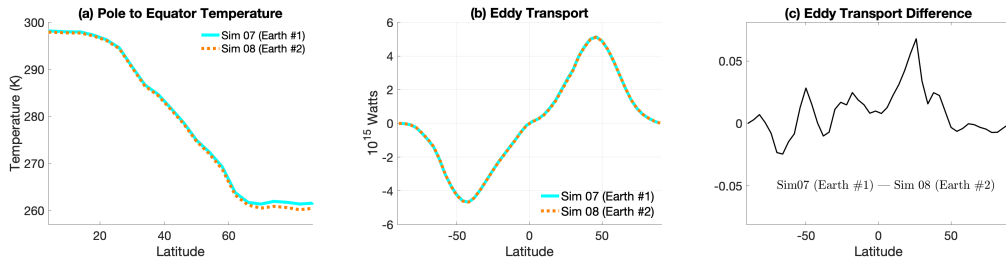
Figure 7. (a) Plotting pole to equator temperature contrast in Kelvin as per Figure 5 in Showman et al. (2013). (b) Eddy energy fluxes for simulation 07 (Earth #1) and simulation 08 (Earth #2) and (c) their difference.
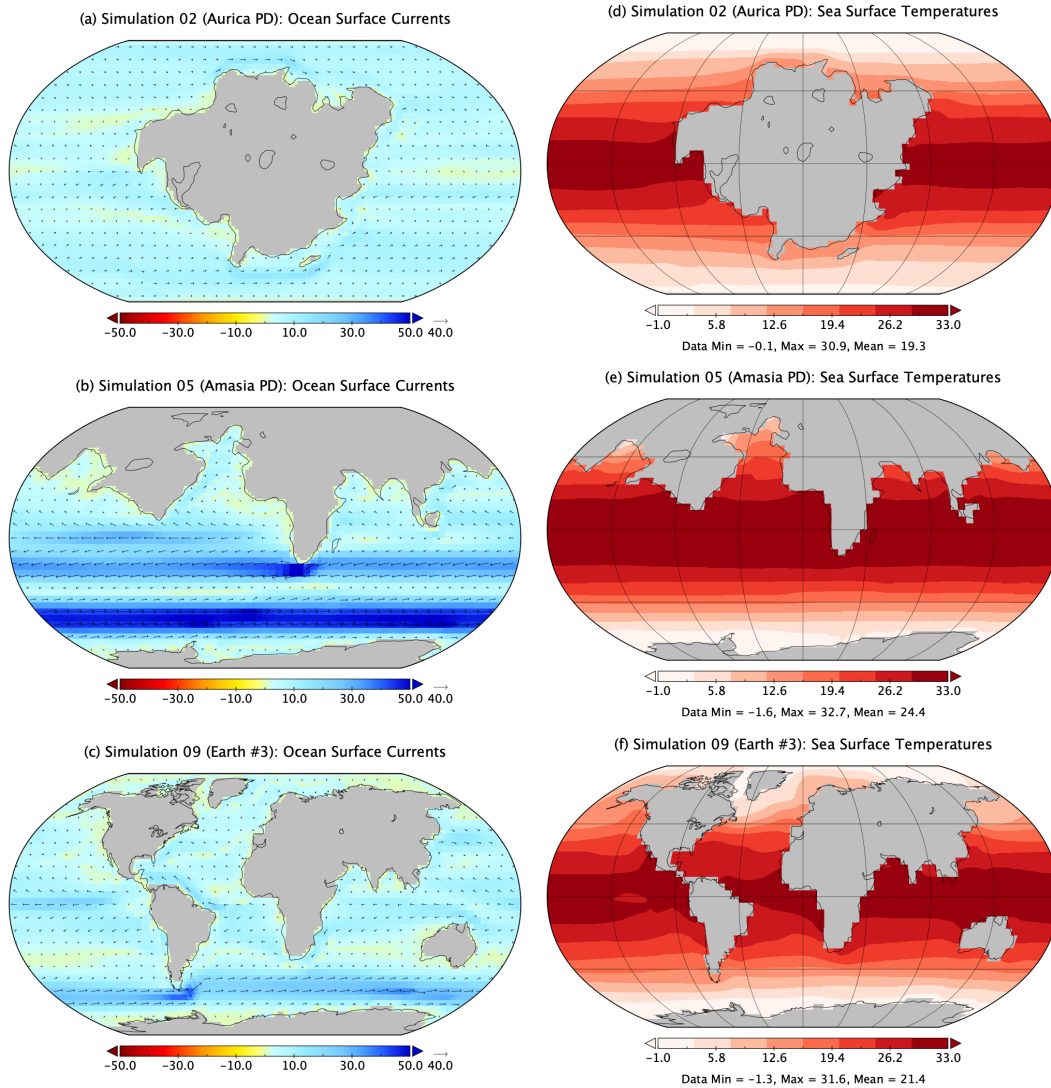
Figure 8. Ocean heat transport in first layer of the ocean (a b c) and sea surface temperatures (d e f) for Aurica PD (sim 02), Amasia PD (sim 05) and (EarthNoAer_NoO3_Rot_Ins) (sim 09).

This increase in land masses at northerly latitudes means that there is less ocean heat transport to melt the ice in the northern hemisphere summers as happens on modern Earth. Some of the heating differences can be seen in the middle right panel of Figure S2 where the oceanic meridional transport for the modern Earth simulations (07–09) is lower at lower latitudes than the Amasia simulations (04–06). This is because there are no southern low latitude continents (e.g. S. America or S. Africa) and the northern hemisphere continents are now pushed to higher northern latitudes in the Amasia runs. At the same time in Figure S4 we see that there are active ocean currents in the modern Earth sim 09 (bottom panels) near the northern polar regions (and in the Aurica sims at high latitudes - top panels), but none are possible in the Amasia sim 05 run (middle panels).

The lack of a northern polar ocean means that more ice resides on land and in lakes all year round near the north pole, as we see in present day Antarctica, for the three Ama-

sia simulations . This is the well known ice-albedo climate feedback and explains why the Amasia simulations tend to be cooler than the Aurica ones. Simulation 05 (Amasia PD) is the coolest of the Amasia simulations. This is because its mean topographic height is higher (especially near the north polar regions) than in (sims 04 and 06). See Figure S5e versus S5d and S5f. The higher relief means simulation 05's lapse rate is lower on average and as discussed in the Methods section above it is cooler and hence instead of rainfall we tend to get snowfall at high latitudes. This fact is also born out in Figure 2 where grid snow+ice fractional amounts are quite high in the northern hemisphere winter months (top center) and southern hemisphere winter months (bottom center) in comparison with the modern Earth simulation 09 with the same rotation rate and insolation. Note that Sim 09 coverage on Greenland in the northern hemisphere summer. This is because we have not adjusted the height of Greenland assuming it no longer has an ice sheet, so it will accumulate snow and maintain it because of its higher altitude. In reality it would likely not be snow covered at this higher insolation as its topographic height would surely be far lower, although one would also have to consider the effects of any land rebound height from the removal of the ice sheets.

It is informative to contrast simulation 02 (Aurica PD) with simulation 05 (Amasia PD). Simulation 02 has land at lower latitudes and uses the same "present day" (PD) topographic height values for inputs as simulation 05 where the landmasses reside at high latitudes. In Table 1 we give their mean surface temperatures, planetary albedo, fractional snow & ice coverage and "Habitable Fraction." The snow & ice coverage as illustrated in Figure 2 is clearly related to the planetary albedo and mean surface temperatures in Table 1. In Table 1 it is clear that the snow & ice fractions are much higher for the Amasia runs (04–06) compared to the Aurica runs (01–03), and highest for simulation 05 in particular. Simulation 05 has the highest snow fraction amount corresponding directly to the lowest mean surface temperature of simulations 01–06. This coldest of the future climates (sim 05) is nearly 1°C cooler than its corresponding modern Earth-like simulation (09). We see a lower fractional snow+ice coverage for simulation 09 in Figure 2 versus that of simulation 05. This in turn is related to the fact that simulation 09 maintains open ocean at northern pole which prevents the year round land ice seen in simulation 05 (see Figure S4). Hence simulation 05 has 10.2% for the snow+ice versus a mere 6.4% for simulation 09 at the same rotation and insolation.

The general effect of the different land/sea masks between simulations 01–03 and 04–06 and how they compare with the modern Earth-like mask in simulations 07–09 are seen in Supplementary Material Figures S2 and S3. In Figure S2 The largest differences are seen in the oceanic meridional transport between the Aurica & Earth-like simulations. The weaker values seen for simulations 01–03 are likely explained by the large low latitude landmass restricting meridional heat transport over a large longitudinal range (left middle panel). In the right middle panel of Figure S2 we see how having larger low-latitude open-ocean increases the oceanic meridional transport for the Amasia simulations (04–06) versus the modern Earth-like simulations (07–09). Total (atmosphere + ocean) meridional heat transport is very similar between simulations where the only discernible differences manifest themselves in the larger northern hemisphere transport for simulations 07–09 versus 01–03, which certainly related to the differences in oceanic transport as discussed above.

These general trends are repeated in Figure S3 where we plot the stream function which indicates the strength of the Hadley circulation. The Aurica PD (sim 02) stream function is the weaker of the three as we saw in Figure S2 (lower panels). Looking at Amasia (sim 05) versus Earth-like (simulation 09) the northern hemisphere values are very similar, but the southern values differ likely because of the low–mid latitude south American, south African, and Australian continents in simulation 09 that do not exist in simulation 05.

Work by Spiegel et al. (2008) uses a metric of "climatic habitability" that defines the amount of surface area of a planet that can host liquid water (e.g., surface temperatures in the range 0<T<100°C) at modern Earth atmospheric pressures. In the right–most column of Table 1 the left values are given using this metric, while the right values utilize a larger temperature range since life on Earth has been found to thrive in temperatures as high as 121°C and as low as –15°C (e.g. NRC, 2007, Table 3.1). These metrics are calculated from 10 year averages (post-equilibrium) of the ground and sea temperatures. From Table 1 it is clear that the Aurica simulations (01–03) have the largest surface habitable fraction amongst all of the simulations. Since none of our simulations approach the boiling part of water in any region this is clearly due to the high-latitude continents found in simulations (04–09) that manifest below freezing temperatures not widely present in (sims 01-03). (sims 07 & 08) have large areas with temperatures below freezing – not unexpected given their lower insolations What is perhaps most surprising are the values for Amasia PD (sim 05) which are lower than the Earth simulations (07 & 08) at lower insolation. As noted above, this is attributable to the large ice sheets in the high latitude northern and southern hemispheres. Even though simulation 05 has a higher mean surface temperature than simulations 07–08 the higher global snow fraction appears to influence this metric more than may be expected. However, caution is warranted when using this habitabilty metric as other work (e.g. Sparrman, 2021) has shown that applying the Spiegel et al. (2008) temperature definition in a 3–D sense reveals little difference in "climatic habitability" between worlds that otherwise appear quite climatically distinct. On Earth life has been found to withstand pressures beyond those of deep sea trenches on Earth (e.g. Sharma et al., 2002; Vanlint et al., 2011), at the bottom of thick ice sheets (e.g. Griffiths et al., 2021) and in extremely deep mines (e.g. Lollar et al., 2019; Drake et al., 2021). Given enough time life has found a way to fill nearly every ecological niche on the modern Earth. While a habitability metric like that used herein may be imperfect it can still provide us a simple way to compare the surface climates of different worlds.

4 Conclusions

The supercontinents of the future can provide us some guidance on how surface temperatures will increase or decrease depending on how the continents are distributed, with implications for exoplanet climate and habitability. But there are other factors to consider related to weathering rates and volcanic outgassing (e.g. Jellinek et al., 2019), not to mention the related role of atmospheric pressure (Gaillard & Scaillet, 2014). We have also used a fixed atmospheric CO_2 concentration in this paper to avoid introducing a further parameter that can add climate variability and, interesting as it would be, exploring the climate with a dynamic carbon cycle is left for future work.

The 30 minute increase in the length of day between simulations 07 and 08 appears to play little to no role in the climate dynamics as there is little discernible difference in the strength or distribution of the Hadley or eddy transport diagnostics. This implies the same for simulations 01–06 with their 30 min longer day lengths than present day Earth.

While we discuss the future climate of Earth we do not touch on the future of life. There are too many uncertainties for us to speculate, but recent work provides some guidelines (Mello & Friaça, 2019). The reduced tides during the supercontinent stage (Davies et al., 2020) will lead to reduced vertical mixing rates, i.e. a reduced vertical diffusivity in the abyssal ocean (Munk, 1966; Wunsch & Ferrari, 2004). This may have implications for ocean ecosystems, and biodiversity. At the same time it appears that the formation of Pangea had little effect on the global biodiversity of marine animals (Zaffos & Peters, 2017) and Pangea was in a very weak tidal state (Green et al., 2017).

It would be interesting to compare the GCM derived climates for the supercontinent at low latitude in the Aurica runs with previous work on Pangea (e.g. Chandler et al., 1992; Chandler, 1994; Fluteau et al., 2001; Gibbs et al., 2002; Roscher et al., 2011). Unfortunately it is difficult to make a proper comparison for a number of reasons. First, all of these previous works use either atmosphere only GCMs (i.e., no ocean) or shallow mixed layer oceans with either prescribed horizontal heat transport or none at all. Secondly, unlike Aurica, Pangea spanned not only lower latitudes (like Aurica), but also high southern latitudes where ice/snow forms easily (e.g. Chandler et al., 1992, Figure 5). Finally, there are different reconstructions for different time periods and not all are directly comparable to those we simulate herein. This makes a direct comparison with Pangea complicated and we leave such an analysis for the future.

These new reconstructions may prove useful for exoplanetary where researchers will have a larger library of topographies and land/sea masks to chose from when estimating the probability of surface habitability on neighboring worlds.

References

Argus, D. F., Peltier, W. R., Drummond, R., & Moore, A. W. (2014, 05). The Antarctica component of postglacial rebound model ICE-6G_C (VM5a) based on GPS positioning, exposure age dating of ice thicknesses, and relative sea level histories. *Geophysical Journal International*, *198*(1), 537-563. Retrieved from https://doi.org/10.1093/gji/ggu140 doi: 10.1093/gji/ggu140

Barker, P. F. (2001). Scotia sea regional tectonic evolution: implications for mantle flow and palaeocirculation. *Earth-Science Reviews*, *55*, 1-39.

Bills, B. G., & Ray, R. D. (1999). Lunar orbital evolution: A synthesis of recent results. *Geophysical Research Letters*, *26*(19), 3045–3048.

Chandler, M. A. (1994, 01). Depiction of modern and Pangean deserts: Evaluation of GCM hydrological diagnostics for paleoclimate studies. In *Pangea: Paleoclimate, Tectonics, and Sedimentation During Accretion, Zenith, and Breakup of a Supercontinent.* Geological Society of America. Retrieved from https://doi.org/10.1130/SPE288-p117 doi: 10.1130/SPE288-p117

Chandler, M. A., Rind, D., & Ruedy, R. (1992, 05). Pangaean climate during the Early Jurassic: GCM simulations and the sedimentary record of paleoclimate. *GSA Bulletin*, *104*(5), 543-559. Retrieved from https://doi.org/10.1130/0016-7606(1992)104<0543:PCDTEJ>2.3.CO;2 doi: 10.1130/0016-7606(1992)104⟨0543:PCDTEJ⟩2.3.CO;2

Claire, M. W., Sheets, J., Cohen, M., Ribas, I., Meadows, V. S., & Catling, D. C. (2012, September). The Evolution of Solar Flux from 0.1 nm to 160 μm: Quantitative Estimates for Planetary Studies. *The Astrophysical Journal*, *757*, 95. doi: 10.1088/0004-637X/757/1/95

Collins, M., Knutti, R., Arblaster, J., Dufresne, J.-L., Fichefet, T., Friedling-stein, P., . . . Wehner, M. (2013). Long-term Climate Change: Projections, Commitments and Irreversibility. *Climate Change 2013: The Physical Science Basis. Contribution of Working Group I to the Fifth Assessment Report of the Intergovernmental Panel on Climate Change*, 1029–1136. doi: 10.1017/CBO9781107415324.024

Davies, H. S., Green, J. A. M., & Duarte, J. C. (2018). Back to the future: Testing different scenarios for the next supercontinent gathering. *Global Planetary Change*, *169*, 133–144.

Davies, H. S., Green, J. A. M., & Duarte, J. C. (2019). Back to the future ii: Four views of future tides. *Earth System Dynamics*, *11*, 291–299.

Davies, H. S., Mattias Green, J. A., & Duarte, J. C. (2020, March). Back to the future II: tidal evolution of four supercontinent scenarios. *Earth System Dynamics*, *11*(1), 291-299. doi: 10.5194/esd-11-291-2020

DeConto, R. M., & Pollard, D. (2003). Rapid Cenozoic glaciation of Antarctica induced by declining atmospheric CO2. *Nature*, *421*, 245–249.

Del Genio, A. D., Way, M. J., Kiang, N. Y., Aleinov, I., Puma, M. J., & Cook, B. (2019, December). Climates of Warm Earth-like Planets. III. Fractional Habitability from a Water Cycle Perspective. *The Astrophysical Journal*, *887*(2), 197. doi: 10.3847/1538-4357/ab57fd

Drake, H., Roberts, N. M. W., Reinhardt, M., Whitehouse, M., Ivarsson, M., Karlsson, A., . . . Kielman-Schmitt, M. (2021, 6). Biosignatures of ancient microbial life are present across the igneous crust of the Fennoscandian shield. *Communications Earth & Environment*, *2*(102), 1. Retrieved from https://doi.org/10.1038/s43247-021-00170-2 doi: 10.1038/s43247-021-00170-2

Duarte, J. C., Schellart, W. P., & Rosas, F. M. (2018). The future of Earth's oceans: Consequences of subduction initiation in the Atlantic and implications for supercontinent formation. *Geological Magazine*, *155*(1), 45–58. doi: 10.1017/S0016756816000716

Dunne, E. M., Farnsworth, A., Greene, S. E., Lunt, D. J., & Butler, R. J. (2021). Climatic drivers of latitudinal variation in Late Triassic tetrapod diversity. *Paleontology*, *64*, 101-117.

Farnsworth, A., Lunt, D., O'Brien, C., Foster, G., Inglis, G., Markwick, P., . . . Robinson, S. (2019). Climate sensitivity on geological timescales controlled by non-linear feedbacks and ocean circulation. *Geophysical Research Letters*, 2019GL083574.

Fluteau, F., Besse, J., Broutin, J., & Ramstein, G. (2001). The late permian climate. what can be inferred from climate modelling concerning pangea scenarios and hercynian range altitude? *Palaeogeography, Palaeoclimatology, Palaeoecology*, *167*(1), 39 - 71. Retrieved from http://www.sciencedirect.com/science/article/pii/S0031018200002303 doi: https://doi.org/10.1016/S0031-0182(00)00230-3

Franck, S., Kossacki, K., & Bounama, C. (1999, July). Modelling the global carbon cycle for the past and future evolution of the earth system. *Chemical Geology*, *159*(1-4), 305-317. doi: 10.1016/S0009-2541(99)00043-1

Gaillard, F., & Scaillet, B. (2014, Oct). A theoretical framework for volcanic degassing chemistry in a comparative planetology perspective and implications for planetary atmospheres. *Earth and Planetary Science Letters*, *403*, 307-316. doi: 10.1016/j.epsl.2014.07.009

Gibbs, M. T., Rees, P. M., Kutzbach, J. E., Ziegler, A. M., Behling, P. J., & Rowley, D. B. (2002). Simulations of permian climate and comparisons with climate-sensitive sediments. *The Journal of Geology*, *110*(1), 33-55. Retrieved from https://doi.org/10.1086/324204 doi: 10.1086/324204

Green, J. A. M., Huber, M., Waltham, D., Buzan, J., & Wells, M. (2017). Explicitly modelled deep-time tidal dissipation and its implication for lu-

nar history. *Earth and Planetary Science Letters*, *461*, 46–53. doi: 10.1016/j.epsl.2016.12.038

Green, J. A. M., Molloy, J. L., Davies, H. S., & Duarte, J. C. (2018). Is there a tectonically driven supertidal cycle? *Geophysical Research Letters*, *45*, 3568–3576. doi: 10.1002/2017GL076695

Griffiths, H. J., Anker, P., Linse, K., Maxwell, J., Post, A. L., Stevens, C., . . . Smith, J. A. (2021). Breaking all the rules: The first recorded hard substrate sessile benthic community far beneath an antarctic ice shelf. *Frontiers in Marine Science*, *8*, 76. Retrieved from https://www.frontiersin.org/article/10.3389/fmars.2021.642040 doi: 10.3389/fmars.2021.642040

Huber, B. T., MacLeod, K. G., Watkins, D. K., & Coffin, M. F. (2018). The rise and fall of the cretaceous hot greenhouse climate. *Global and Planetary Change*, *167*, 1 - 23. doi: https://doi.org/10.1016/j.gloplacha.2018.04.004

Jellinek, M., Lenardic, A., & Pierrehumbert, R. (2019, 06). Ice, fire or fizzle: The climate footprint of earth's supercontinental cycles. *Geochemistry, Geophysics, Geosystems*, 10.

Krijgsman, W., Hilgen, F. J., Raffi, I., Sierro, F. J., & Wilson, D. S. (1999). Chronology, causes and progression of the Messinian salinity crisis. *Nature*, *400*(6745), 652–655.

Lollar, G. S., Warr, O., Telling, J., Osburn, M. R., & Lollar, B. S. (2019). 'follow the water': Hydrogeochemical constraints on microbial investigations 2.4 km below surface at the kidd creek deep fluid and deep life observatory. *Geomicrobiology Journal*, *36*(10), 859-872. Retrieved from https://doi.org/10.1080/01490451.2019.1641770 doi: 10.1080/01490451.2019.1641770

Mello, F. d. S., & Friaça, A. C. S. (2019). The end of life on earth is not the end of the world: converging to an estimate of life span of the biosphere? *International Journal of Astrobiology*, 1-18. doi: 10.1017/S1473550419000120

Mitchell, R. N., Kilian, T. M., & Evans, D. A. D. (2012). Supercontinent cycles and the calculation of absolute palaeolongitude in deep time. *Nature*, *482*, 208–211.

Montes, C., Cardona, A., Jaramillo, C., Pardo, A., Silva, J. C., Valencia, V., . . . Niño, H. (2015). Middle Miocene closure of the Central American Seaway. *Science*, *348*, 226–229.

Munk, W. H. (1966). Abyssal recipes. *Deep-Sea Research and Oceanographic Abstracts*, *13*(4), 707–730. doi: 10.1016/0011-7471(66)90602-4

NRC. (2007). *The limits of organic life in planetary systems*. Washington, DC: The National Academies Press. Retrieved from https://www.nap.edu/catalog/11919/the-limits-of-organic-life-in-planetary-systems doi: 10.17226/11919

Ozaki, K., & Reinhard, C. T. (2021, January). The future lifespan of Earth's oxygenated atmosphere. *Nature Geoscience*, *14*(3), 138-142. doi: 10.1038/s41561-021-00693-5

Parrish, J. (1993, 03). Climate of the supercontinent pangea. *Journal of Geology*, *101*, 215-233. doi: 10.1086/648217

Pastor-Galán, D., Nance, R. D., Murphy, J. B., & Spencer, C. J. (2019). Supercontinents: myths, mysteries, and milestones. *Geological Society, London, Special Publications*, *470*(1), 39–64. Retrieved from https://sp.lyellcollection.org/content/470/1/39 doi: 10.1144/SP470.16

Peltier, W. R., Argus, D. F., & Drummond, R. (2015). Space geodesy constrains ice age terminal deglaciation: The global ice-6g_c (vm5a) model. *Journal of Geophysical Research: Solid Earth*, *120*(1), 450-487. Retrieved from https://agupubs.onlinelibrary.wiley.com/doi/abs/10.1002/2014JB011176 doi: https://doi.org/10.1002/2014JB011176

Pierrehumbert, R. T., Abbot, D. S., Voigt, A., & Koll, D. (2011). Climate of the neoproterozoic. *Annual Reviews of Earth and Planetary Sciences*, 417-460.

Ramstein, G. (2011, September). Climates of the Earth and Cryosphere Evolution. *Surveys in Geophysics*, *32*(4-5), 329-350. doi: 10.1007/s10712-011-9140-4

Roscher, M., Stordal, F., & Svensen, H. (2011). The effect of global warming and global cooling on the distribution of the latest permian climate zones. *Palaeogeography, Palaeoclimatology, Palaeoecology*, *309*(3), 186 - 200. Retrieved from http://www.sciencedirect.com/science/article/pii/S0031018211002987 doi: https://doi.org/10.1016/j.palaeo.2011.05.042

Sagan, C., & Mullen, G. (1972, July). Earth and Mars: Evolution of Atmospheres and Surface Temperatures. *Science*, *177*(4043), 52-56. doi: 10.1126/science.177.4043.52

Schmittner, A., Silva, T. A. M., Fraedrich, K., Kirk, E., & Lunkeit, F. (2011). Effects of Mountains and Ice Sheets on Global Ocean Circulation. *Journal of Climate*, *24*, 2814–2829.

Sharma, A., Scott, J. H., Cody, G. D., Fogel, M. L., Hazen, R. M., Hemley, R. J., & Huntress, W. T. (2002). Microbial activity at gigapascal pressures. *Science*, *295*(5559), 1514–1516. Retrieved from https://science.sciencemag.org/content/295/5559/1514 doi: 10.1126/science.1068018

Showman, A. P., Wordsworth, R. D., Merlis, T. M., & Kaspi, Y. (2013). Atmospheric Circulation of Terrestrial Exoplanets. In S. J. Mackwell, A. A. Simon-Miller, J. W. Harder, & M. A. Bullock (Eds.), *Comparative climatology of terrestrial planets* (p. 277). doi: 10.2458/azu_uapress_9780816530595-ch12

Smith, A. G., & Pickering, K. T. (2003). Oceanic gateways as a critical factor to initiate icehouse Earth. *Journal of the Geological Society, London*, *160*, 337-340.

Sparrman, V. (2021). Estimates of fractional habitability for proxima centauri b using a 3d gcm. *Dissertation*, *1*, 1–16. Retrieved from http://urn.kb.se/resolve?urn=urn:nbn:se:uu:diva-415703

Spiegel, D. S., Menou, K., & Scharf, C. A. (2008, July). Habitable Climates. *The Astrophysical Journal*, *681*(2), 1609-1623. doi: 10.1086/588089

Tada, R., Zheng, H., & Clift, P. D. (2016). Evolution and variability of the Asian monsoon and its potential linkage with uplift of the Himalaya and Tibetan Plateau. *Progress in Earth and Planetary Science*, *3*, 4.

Vanlint, D., Hazael, R., Bailey, E., Meersman, F., McMillan, P., Michiels, C., & Aertsen, A. (2011, 12). Rapid acquisition of gigapascal-high-pressure resistance by escherichia coli. *mBio*, *2*, e00130-10. doi: 10.1128/mBio.00130-10

Way, M. J., Aleinov, I., Amundsen, D. S., Chandler, M. A., Clune, T. L., Del Genio, A. D., ... Tsigaridis, K. (2017, July). Resolving Orbital and Climate Keys of Earth and Extraterrestrial Environments with Dynamics (ROCKE-3D) 1.0: A General Circulation Model for Simulating the Climates of Rocky Planets. *Astrophysical Journal Supplement Series*, *231*, 12. doi: 10.3847/1538-4365/aa7a06

Way, M. J., Del Genio, A. D., Aleinov, I., Clune, T. L., Robinson, T. D., Kelly, M., & Kiang, N. Y. (2018). Climates of warm earth-like planets. i. 3d model simulations. *The Astrophysical Journal Supplement Series*, *239*(2).

Wunsch, C., & Ferrari, R. (2004). Vertical mixing, energy, and the general circulation of the oceans. *Annual Review of Fluid Mechanics*, *36*(1), 281–314.

Yang, J., Boué, G., Fabrycky, D. C., & Abbot, D. S. (2014). Strong dependence of the inner edge of the habitable zone on planetary rotation rate. *Astrophysical Journal Letters*, *787*(1). doi: 10.1088/2041-8205/787/1/L2

Yoshida, M. (2016, 09). Formation of a future supercontinent through plate motion–driven flow coupled with mantle downwelling flow. *Geology*, *44*(9), 755-758. Retrieved from https://doi.org/10.1130/G38025.1 doi: 10.1130/G38025.1

Yoshida, M., & Santosh, M. (2018). Voyage of the indian subcontinent since pangea breakup and driving force of supercontinent cycles: Insights on dynamics from numerical modeling. *Geoscience Frontiers*, *9*(5), 1279 - 1292. Retrieved from

586   `http://www.sciencedirect.com/science/article/pii/S1674987117301536`

587   (SPECIAL ISSUE: Frontiers in geoscience:A tribute to Prof. Xuanxue Mo)

588   doi: https://doi.org/10.1016/j.gsf.2017.09.001

589   Zaffos, S., A. Finneganb, & Peters, S. E.   (2017).   Plate tectonic regulation of

590   global marine animal diversity.   *PNAS*, *114*(22), 5653–5658.   Retrieved from

591   `https://www.pnas.org/content/114/22/5653`   doi: https://doi.org/10.1073/

592   pnas.1702297114